Processing body dynamics drive non-genetic MEK inhibitors tolerance by fine-tuning KRAS and NRAS translation

Olivia Vidal-Cruchez[1,2], Victoria J Nicolini[1,2], Tifenn Rete[1,2], Roger Rezzonico[2,3], Caroline Lacoux[4], Julien Fassy[4], Karine Jacquet[1,2], Marie-Angela Domdom[1,2], Chloé Ventujol[1,2], Thierry Juhel[1,2], Barnabé Roméo[1,2], Jérémie Roux[1,2], Arnaud Hubstenberger[5], Bernard Mari[2,4], Baharia Mograbi[1,2,*], Paul Hofman[1,2,6,*], Patrick Brest[1,2,$]

1. Université Côte d'Azur, Institute of Research on Cancer and Aging of Nice (IRCAN), CNRS, Inserm, Centre Antoine Lacassagne, Nice, France
2. FHU-OncoAge, Nice, France
3. Université Côte d'Azur, Institut de Pharmacologie Moléculaire et Cellulaire (IPMC), INSERM, CNRS, Sophia Antipolis, France
4. Université Côte d'Azur, Institut de Pharmacologie Moléculaire et Cellulaire (IPMC), CNRS, Sophia Antipolis, France
5. Université Côte d'Azur, Institut Biologie Valrose (IBV), CNRS, Inserm, Nice, France
6. Université Côte d'Azur, CHU-Nice, Pasteur Hospital, Laboratory of Clinical and Experimental Pathology, FHU OncoAge, Hospital-Integrated Biobank (BB-0033-00025), Nice, France

*Equal contribution

$ Corresponding author: Brest Patrick, Université Côte d'Azur, IRCAN, 28, Avenue de Valombrose, Nice, France. Patrick.BREST@univ-cotedazur.fr

Abstract

Background

Overactivation of the Mitogen-activated protein kinase (MAPK) pathway is a critical driver of many human cancers. However, therapies that target this pathway have only been effective in a few cancers, as cancers inevitably end up developing resistance. Puzzling observations have suggested that MAPK targeting in tumor fails because of an early compensatory RAS overexpression, but through unexplained mechanisms.

Methods

Lung, breast, and melanoma cancer cells were incubated with MEK inhibitors (MEKi). Kinetics of expression of KRAS, NRAS mRNA and proteins and processing bodies (PBs) proteins were followed overtime by immunoblot and confocal studies.

Results

Here, we identified a novel mechanism of drug tolerance for MEKi involving PBs essential proteins like DDX6 or LSM14A. MEKi promoted the translation of KRAS and NRAS oncogenes, which in turn triggered BRAF phosphorylation. This overexpression, which occurred in the absence of neo-transcription, depended on PBs dissolution as a source of RAS mRNA reservoir. In addition, in response to MEKi removal, we showed that the process was dynamic since the PBs quickly reformed, reducing MAPK signaling. These results underline a dynamic spatiotemporal negative feedback loop of MAPK signaling via RAS mRNA sequestration. Furthermore, in long-tolerant cells, we observed a LSM14A loss of expression that promoted a low PBs number phenotype together with strong KRAS and NRAS induction capacities.

Conclusions

Altogether we describe here a new intricate mechanism involving PB, DDX6 and LSM14A in the translation regulation of essential cellular pathways that pave the way for future therapies altering PBs dissolution to improve cancer targeted-drug therapies.

Keywords

RAS, KRAS, NRAS, MAPK, Liquid Liquid phase separation, DDX6, processing bodies, oncogene, MEKi.

Background

mRNAs are actively translated, repressed, stored, or degraded in response to environmental cues. These post-transcriptional pathways are critical for controlling cell fates that are altered in pathological conditions, such as cancers[1,2]. In this regard, recent transcriptome-wide studies have revealed that most RNAs have a restricted, dynamic, and regulated subcellular localization. From the key players of this process emerge two RNAs clusters and associated regulatory RNA binding proteins (RBP), known as the constitutive processing bodies (PBs) and environmentally-induced stress granules[3,4]. In contrast to organelles with a lipid bilayer membrane, membraneless structures are formed through a process known as liquid-liquid phase separation (LLPS) that confers a wide range of plasticity to these super-assemblies[5]. Sequestration of mRNAs into these ribonucleoprotein granules is associated with translational repression, thus uncoupling mRNA expression from protein production, and enabling the spatiotemporal control of gene expression[3]. Furthermore, PBs and stress granules act as reservoirs of silent mRNAs that can re-enter translation to adapt protein expression to the environment, providing plasticity to the genetic program[3,5–7]. Although, this post-transcriptional control is key to cellular adaptation in inconstant and stressful environments[1], few studies have investigated the role of PBs in the context of cancer progression and particularly for the emergence of drug-tolerant cells.

Mitogen-activated protein kinase (MAPK) pathways represent ubiquitous signal transduction pathways that control cell fates by phosphorylating hundreds of substrates. The RAS-RAF-MEK-ERK pathway is altered in ~40% of all human cancers, mainly due to RAS oncogenic mutations (32%) and its downstream effector BRAF (~10%). KRAS is mainly found mutated in pancreatic cancer (88%), lung cancer (30%), and colorectal

adenocarcinoma (50%). NRAS and BRAF are modified in melanoma (17% and 55% respectively), thyroid carcinoma (19% and 55% respectively), and lung cancer (1% and 5% respectively)[8,9]. Given the causative role of the RAS-RAF-MEK-ERK pathway hyperactivation in driving tumorigenesis, several MEK, BRAF, and KRAS inhibitors (MEKi, BRAFi, and KRASi respectively) were developed over the last decades [10–12]. Unfortunately, these treatments are inevitably associated with drug tolerance, acquired resistance, and tumor relapse[10,13].

Even if a part of the resistance is directly attributable to somatic mutation acquisition, the early drug resistance arose from plastic drug-tolerant or persister cells. Among these non-genetic early resistance events, the upregulation of KRAS and NRAS proteins in response to BRAFi or MEKi targeting the pathway downstream was suggested as a possible contributor[14,15], while the underlying mechanism remains unknown. Employing a combination of genetic and pharmacological approaches, we demonstrate herein that PBs are associated with drug tolerance through a DDX6-dependent negative feedback loop that fine-tunes KRAS and NRAS expression by controlling mRNA translation.

Material and methods

Cell culture.

The A549, H1650, Mel501, BT549 were cultured according to the recommendations of the ATCC. A549 (human lung adenocarcinoma epithelial cell line, ATCC, number CCL-185) and Mel-501(melanoma epithelial cell line), were grown in Dulbecco's Modified Eagle Medium (DMEM) supplemented with 10% fetal bovine serum (FBS). BT549 (Breast epithelial cell line, ATCC, number HTB-122) was grown in DMEM supplemented with 10% FBS and non-essential amino-acid (Thermofischer). H1650 (human lung adenocarcinoma epithelial cell line, ATCC, number CRL-5908) was grown in Roswell Park Memorial Institute (RPMI)-1640 medium supplemented with 10% FBS, 1mM sodium pyruvate. All the cells were maintained at 37°C in a 5% CO_2 in a humidified incubator. All cells were maintained no more than one month and were identified using STR profile (Eurofins Genomics).

DDX6 and LSM14A GFP stable cell lines.

The pPRIPu GFP-DDX6 plasmid used in this study were constructed as follows:

The pPRIPu CrUCCI vector[16] (kind gift of Dr. F Delaunay) was amplified with primer adaptors for AgeI and BamH1. pEGFP-C1_p54cp (kind gift of Drs D. Weil and M. Kress) were digested by AgeI and BamH1 and the respective resulting fragments were inserted in pPRIPU. The integrity of the entire sequence in the later has been confirmed by sequencing analysis. Briefly, replication-defective, self-inactivating retroviral constructs were used to establish stable A549 cell lines. Selection was performed by puromycin (10µg/ml). Then, the cells were sorted as a polyclonal population and used in the following experiments.

siRNA transient transfection.

Cells were plated at 200 000 cells/well in 6-well plates. After 24h, cells were transfected with siRNA negative Control or Silencer Pre-designed small interfering RNA (siRNA) DDX6, LSM14A, KRAS or NRAS using JetPrime (PolyPlus) according to the manufacturer's instructions as previously described[17]. 48h after transfection, cells were lysed for RNA or protein analysis as described below.

Immunoblotting.

Immunoblotting was performed as described previously[17]. Protein was extracted from cells using Laemmli lysis buffer (12.5mM Na_2HPO_4, 15% glycerol, 3% sodium dodecyl sulfate [SDS]). The protein concentration was measured with the DC Protein Assay (BIO-RAD) and 30µg – 50µg of total proteins were loaded onto 7.5% or 12% SDS-polyacrylamide gels for electrophoresis and transferred onto polyvinylidene difluoride membranes (Millipore). After 1h of blocking with 5% bovine serum albumin or non-fat milk prepared in Phosphate-Buffered Saline (PBS)-0.1% Tween-20 buffer, the blots were incubated overnight at 4°C with antibodies (supp table). After 1h of incubation with a horseradish peroxidase-conjugated secondary antibody (1:3000, Promega), protein bands were visualized using an enhanced chemiluminescence detection kit (Millipore) with the imaging system, Syngene Pxi4 (Ozyme).

Isolation of RNA and quantitative real-time RT-PCR analysis.

Total RNA extraction was performed using TRI-reagent (Sigma-Aldrich). Isolation of RNA from cultured cells was performed as described previously[18]. The RNA concentration

was measured by NanoDrop 2000 (Thermo Fisher Scientific). For mRNA, the cDNA strand was synthesized from 500ng of total RNA. Quantification of *KRAS* and *NRAS* and *RPLP0* genes was measured by power-Sybr-green assays with the StepOne™ Real-time PCR System. qPCR Primers are referenced in the supplementary table.

Immunofluorescence and confocal microscopy.

Cells were grown to confluence and fixed in 4% paraformaldehyde for 20min. After fixation, cells were permeabilized with a solution containing 0.3% Triton X-100 for 5min. Then, cells were incubated with primary antibodies (listed in suppl table) overnight at 4°C in humidified chambers in a solution containing 0.03% Triton X-100, 0.2% gelatin and 1% BSA. Cells were washed and incubated with Alexa Fluor-conjugated secondary antibodies (1:500; Molecular Probes) for 1h at room temperature and mounted in ProLong Diamond Reagent with DAPI (Molecular Probes). Images were captured on a Zeiss LSM880 confocal microscope.

Statistical analysis.

Quantitative data were described and presented graphically as medians and interquartiles or means and standard deviations. The distribution normality was tested with the Shapiro's test and homoscedasticity with a Bartlett's test. For two categories, statistical comparisons were performed using the Student's t-test or the Mann–Whitney's test. All statistical analyses were performed by the biostatistician using R.3.2.2 software and Prism8.0.2 program from GraphPad software. Tests of significance was two-tailed and considered significant with an alpha level of $P<0.05$. (Graphically: * for $P<0.05$, ** for $P<0.01$, *** for $P<0.005$).

Polysome gradient.

Subcellular fractionation. All steps of the subcellular fractionation were performed at 4°C. Cells (60-80x10 6 cells) with or without treatment were trypsinized and washed twice with 15 ml of ice-cold PBS by centrifugation. Cell pellets were resuspended in 1 ml of hypotonic Buffer composed of 40mM Tris-HCl, pH 7.5, 10mM KCl, 3mM $MgCl_2$ and 0.2% Nonidet P-40 supplemented with 1mM DTT and 0,5mM phenylmethylsulfonyl fluoride (PMSF). After incubation for 15min on ice, cells were lysed in a Dounce homogenizer with B pestle. The efficiency of cell lysis keeping the nuclei intact was verified by staining with trypan blue under an optical microscope. The cell lysates were spun at 900g for 5min to obtain the cytoplasm (supernatant) and nuclei (pellet) fractions.

Sucrose gradient fractionation. About 10 OD 260nm of cytosolic extracts were loaded on the top of a linear sucrose gradient (10–50%) made in Sucrose Gradient Buffer (25mM Tris-HCl, pH 7.5, 150mM NaCl, 12mM $MgCl_2$, 1mM DTT) in Ultra-Clear ultracentrifugation tubes (Beckman Coulter). The cytosolic fraction samples were fractionated by ultracentrifugation for 2h 45min at 39,000rpm at 4°C in a Beckman Optima ultracentrifuge with SW41 Ti swinging bucket rotor with the following settings: acceleration 9 and deceleration 4. Following ultracentrifugation, the sucrose gradients were fractionated using a Foxy JR fraction collector and monitoring UA-6 UV light (254-nm wavelength) absorbance detector (Teledyne ISCO), obtaining 12 to 14 fractions.

After addition of 0,5mM $CaCl_2$ and 0,2% SDS, the collected fractions were treated with proteinase K (50mg/ml, Sigma) for 30min at 40°C. Then 10pg of an RNA spike-in was added in each fraction to serve as an internal calibrator of RNA extraction and detection. For this, we used an in vitro transcribed RNA encoding the spike protein of SARS-CoV-2.

Total RNA was extracted by vigorous shaking with an equal volume of Tris pH 8,0 saturated phenol, chloroform, isoamyl alcohol mixture (25:24:1, v/v/v) (Sigma-Aldrich), and phase separation was performed by centrifugation at 12,000g for 15min at 4°C. The upper aqueous phase was washed once with an equal volume of chloroform:isoamyl alcohol (24:1, v/v) (Sigma-Aldrich) by vigorous shaking and centrifugation at 12,000g for 15min at 4°C. The aqueous phase was transferred to a fresh tube and the RNA was precipitated overnight at -20°C by mixing with an equal volume of isopropanol, 2ml of glycoblue TM coprecipitant (Thermo Fisher Scientific) and 1/10 volume of 3M Na acetate pH 5.2. RNA was pelleted by centrifugation at 12,000g for 15min at 4°C.

Results

MEKi response promotes KRAS and NRAS translation.

We first confirmed the accumulation of both NRAS and KRAS protein in response to MEKi, PD184352 (CI-1040) and trametinib, in four different cell lines (A549, H1650, Mel501, BT549) regardless of cancer type (lung, breast, melanoma) and oncogenic drivers (KRASG12S, EGFR, BRAFV600E, PTEN respectively) (Fig.1A). In order to analyze whether both KRAS and NRAS proteins were able to activate the downstream BRAF phosphorylation in these conditions (Fig.1B), we used siKRAS and siNRAS, either alone or in combination. Interestingly, we showed here that both KRAS or NRAS drive sustained BRAF phosphorylation in the presence of PD184352. The complete inhibition of BRAF phosphorylation was indeed almost achieved only when both siRNAs were combined (Fig.1B). Altogether, these results highlight that the increase in protein expression of KRAS or NRAS were sufficient to lead to the phosphorylation of BRAF after MEK inhibition.

In this context, we investigated the potential causes of this increase in KRAS and NRAS protein expression. At the transcriptional level, we showed that *KRAS* and *NRAS* mRNA levels were stable under PD184352 treatment (Fig.2A-B). Furthermore, the PD184352-increase in KRAS and NRAS protein levels was maintained in the presence of the transcription inhibitor Actinomycin D (Fig.2C). Taken together, these results strongly support a post-transcriptional mechanism.

Using a ribosome profiling experiment, we showed that *KRAS* and *NRAS* mRNAs shifted from monosome to heavy polysome fractions in the presence of PD184352 (Fig.2D). In order to confirm an increase in translation, we pretreated A549 cells with the proteasome inhibitor MG132, to accumulate proteins by blocking their degradation. In PD184352 and

MG132 treated cells the accumulation of KRAS was stronger than with MG132 alone, confirming an increased translation of *KRAS* mRNA in the presence of PD184352 (Suppl. Fig.1). Altogether, from these results we conclude that the rapid PD184352-induced NRAS and KRAS overexpression relies on an augmentation in translation rather than transcription.

MEK inhibition promotes PBs dissolution.

Since *KRAS* and *NRAS* mRNAs have been reported to be accumulated in PBs[3,19], we hypothesized that KRAS and NRAS overexpression is associated with the *KRAS* and *NRAS* pool of mRNA previously-stored in PBs becoming available for translation. In this context, we analyzed the number and size of cellular PBs in different cancer cell lines. Strikingly, we uncovered a significant decrease in PBs size and number in response to PD184352 and trametinib in all cell types investigated (Fig.3A-F, Suppl. Fig.2). This MEKi-induced reduction was even more potent as early as 8h, showing a PBs dissolution kinetics correlating with the time course of KRAS and NRAS overexpression. At this time point, MEKi had no effect on cell cycle progression, excluding the possibility that PB dissolution was a secondary effect of cell cycle arrest (Fig.3G-I, Suppl. Fig.2). This global decrease in P-body number was neither associated with changes in DDX6 nor LSM14A levels, two proteins required for PBs formation (Fig.3I), nor with stress granules induction (Suppl. Fig.3).

Then, we analyzed the dynamics of PBs formation and KRAS expression. For this purpose, after a 24h treatment with PD184352 to dissolve PBs and induce KRAS and NRAS overexpression, the MEKi was removed, and cells were harvested at different times (Fig.4A). After PD184352 washout, strong activation of ERK was observed and

maintained over 4h, together with a stable expression of both KRAS and NRAS and phosphorylation of BRAF (Fig.4B). At 8h up to 24h, a gradual decrease in KRAS and NRAS expression along with a decrease in BRAF phosphorylation were inversely correlated with an increasing number of PBs over time (Fig.4B-D, Suppl. Fig.4) suggesting stalled translation. The drug removal was followed with a restoration of a growth rate that was comparable to that of untreated cells, showing the rapid adaptability of the cancer cells (Fig 4E). Therefore, our results provide the first evidence that the high plasticity orchestrated by PBs helps to adapt the rate of RAS translation through negative feedback loops. Secondly, we evidenced the ability of this KRAS and NRAS overexpression to trigger BRAF phosphorylation in presence of MEKi. This PBs/RAS balance distinguished the establishment of drug tolerance from the normal cancer cell growth condition.

Next, we wanted to test whether t P-body dissolution and the associated K-Ras and NRAs overexpression could get fixed over prolonged drug selection. In drug-tolerant A549 cells, after tumor cell treatment with PD184352 at 2.5µM for 8 weeks, the drugs were washed out, and the drug tolerant cells were then cultured for an additional 24h in the presence or absence of PD184352. Figure 5 shows that after MEKi washout for 24h, ERK activation was identical to levels observed in normal cells. Strikingly, the PBs number and size were significantly lower than in the control condition, even in single-dose PD184352 treated cells (Fig.5, Suppl. Fig.5). We identified here that LSM14A expression was strongly decreased in long-term MEKi cultured cells, even in absence of MEKi for 24h. Interestingly, at 10µM of PD184352, the KRAS expression was strongly induced in the resistant cells, together with a significant decrease in PBs (Fig.5, Suppl. Fig.5A). This overexpression was strong enough to maintain a residual phosphorylation of ERK that overcame MEKi inhibition. As a mark of non-genetic resistance, these drug-tolerant cells

restored a full growth phenotype 5 days after MEKi removal (Suppl Fig 5B). Altogether, these results indicate that MEKi-induced PBs dissolution is an early event in drug-tolerant cells and that this mechanism is built up overtime as a strategy for maintaining KRAS/NRAS oncogene addiction.

PBs essential component controls KRAS and NRAS expression.

To test a causative role between the translation repression activities of PBs components and KRAS and NRAS expression, we modulated the level of the RNA helicase DDX6 or LSM14A, essential PBs components. Overexpression of GFP-tagged DDX6 increased PBs size and numbers. This significant increase in PBS correlated with decreased KRAS and NRAS expression (Fig.6A-C, Suppl. Fig.6). Of note, under these conditions, *KRAS* and *NRAS* mRNA levels were unchanged, suggesting a mRNA storage (Fig.6D-E). Inversely, silencing of DDX6 or LSM14A induced a complete dissolution of PBs, that was sufficient to trigger alone the overexpression of KRAS and NRAS (Fig.6F-G). Altogether, these results showed that PBs components plays a critical role in the mediation of MEKi-induced RAS overexpression and the establishment of MEKi drug tolerance.

Discussion

For many decades, studies have pointed genetic mutations as the central mechanism of resistance acquisition to targeted therapy [20]. However, growing evidence challenges this consensus, indicating that non-genetic heterogeneity and cell plasticity actively participate in drug tolerance[21–23]. Recently, new profiling techniques, like FATE-seq, have been carried out to dissect the non-genetic mechanisms of resistance[24]. However, it is clear that genetic and non-genetic mechanisms of resistance or drug tolerance are frequently linked and not mutually exclusive[23,25]. Non-genetic resistance is due to the intrinsic plasticity of tumor cells, i.e., the ability to undergo transcriptional and epigenetic reprogramming in response to environmental challenges or upon therapy. In this context, current therapeutic options for BRAFV600E/K patients include MAPK pathway-targeted therapies, which show remarkable efficacy during the first months of treatment[13]. However, most patients treated with a combination of BRAF inhibitor (BRAFi) and MEK inhibitor (MEKi) inevitably relapse within months[13,26]. This relapse has been highlighted by the presence of so-called persister, cancer stem, drug-tolerant or resistant cells, as reported by different studies that either harbor a genetic or non-genetic program for survival[22,27].

Here, we focused on the early events of drug tolerance. We showed that within 8h, cells were able to set up an overexpression of KRAS and NRAS that was independent of *de novo* transcription and inhibition of protein degradation. Interestingly, we observed that this overexpression persisted over weeks, eventually overcoming MAPK inhibition. The drug-tolerant cells, cultured for long periods in the presence of MEKi, were associated with persistent PBs decrease even 24h following treatment washout, while the restoration of PBs to normal levels could be found in drug-tolerant cells after a short exposure to

MEKi. Continuous versus intermittent BRAF and MEK inhibition in melanoma patients harboring BRAF V600E/K mutations has been tested in a randomized, open-label, phase 2 clinical trial (NCT02196181)[26]. In this study, continuous dosing yielded to a statistically significant improvement in post-randomization progression-free survival compared with intermittent dosing, suggesting that drug-tolerant cancer cells with enhanced plasticity may grow faster after intermittent dosing than long term resistant cells. Moreover, by showing that both KRAS and NRAS are equally important for sustaining BRAF activity, we revealed a new range of possibilities to overcome MAPKi treatments like with the development of KRAS G12C inhibitors resistance in patients harboring either *KRAS* or *NRAS* mutations[11].

We also showed that both PD184352 and trametinib MEKi can dissolve PBs. The involvement of MAPK pathway is consistent with a previous study showing that MAPK3 (ERK1) was associated with PBs dissolution in the absence of DDX6 decrease in a 1,354 human genes siRNA screening[28]. Here, our work highlights the fact that it is the activity rather than the level of ERK that is key for PBs dissolution. However, since ERKs are able to phosphorylate more than 200 intracellular targets, more studies are necessary to determine whether the formation of PBs is dependent on ERK activity, either through direct targeting of PBs components or indirectly through a partner of PBs.

Finally, we showed here that the expression of the PBs component DDX6, a helicase associated with miRNA-dependent repression of translation and PBs storage, conntrol KRAS and NRAS transaltion. These results are consistent with previous studies showing an accumulation of *KRAS* and *NRAS* mRNAs in PBs[3,19], likely dependent on several *let-7* miRNA response-elements on both 3'UTR[29]. In addition, several features of *KRAS* and *NRAS* mRNAs (i.e. the 5.3kb and 4.3kb respective length and the low-GC content of

their coding region or 3'UTR mRNA, 38% and 44% respectively) may also contribute to their targeting to PBs[30]. Of note, previous studies have shown that *KRAS* is poorly translated compared to *HRAS* due to enrichment in genomically underrepresented or rare codons[31,32]. In our study, we observed that either MEKi-induced dissolution or DDX6 or LSM14A downregulation were associated with potent translation in polysome fractions of *KRAS* and *NRAS* mRNAs and with their respective protein overexpression. These results suggest that rare codons, which are often associated with the presence of AU-rich third codon, may favor the recruitment of mRNA repressors due to low-speed translation processing that can however be overcome in specific conditions.

Conclusion

Collectively, these results reveal a new negative feedback loop involving PBs in the translational control of *KRAS* and *NRAS* mRNAs (Suppl Fig. 7). This type of regulation of MAPK pathway we described here should pave the way for targeted therapies to avert early resistance and target drug-tolerant cells before relapse.

Ethics approval and consent to participate

Not applicable

Consent for publication

Not applicable

Availability of data and materials

Data sharing not applicable to this article as no datasets were generated or analyzed during the current study. Necessary and reasonable information could be obtained from the corresponding author.

Competing interests

The authors declare no financial relationships with any organizations that might have an interest in the submitted work over the previous three years and no other relationships or activities that could appear to have influenced the submitted work.

Funding

Authors acknowledged from the French Government (Agence Nationale de Recherche, ANR) through the 'Investments for the Future' LABEX SIGNALIFE (ANR-11-LABX-0028-01 and IDEX UCAJedi ANR-15-IDEX-01), ANR FibromiR N° ANR-18-CE92-0009-01; “Fondation ARC pour la Recherche contre le Cancer” (Canc’air GENExposomics and PJA-20191209562), Canceropole PACA; DREAL PACA, ARS PACA, Région Sud, Institut National du Cancer, INSERM cancer; ITMO Cancer 2014-2019 (14APS001MCSR and 18CN045). The authors greatly acknowledge the IRCAN’s Flow Cytometry Facility

(CytoMed) and the IRCAN's Molecular and Cellular Core Imaging (PICMI) Facility that were supported by le FEDER, Ministère de l'Enseignement Supérieur, Conseil régional Provence Alpes-Côte d'Azur, Conseil Départemental 06, ITMO Cancer Aviesan (plan cancer), Gis Ibisa, Cancéropole PACA, le CNRS and Inserm

Authors' contributions

OVC and PB supervised and wrote the manuscript. OVC, VJN, TR, RR, CL JF, KJ, MAD, CV, TJ, and BR have made substantial contributions to the conception, the design of the work; the acquisition, analysis, and the interpretation of data. JR, AH, BMa, BMo, PH substantively revised the manuscript. AH, BMa, BMo, PH and PB supported the work through fundings. All authors read and approved the final manuscript.

Acknowledgments

Our thanks to the UCA Office of International Scientific Visibility for comments on the English version of the manuscript. Authors would like to thank Dr Julien Cherfils and Ludovic Cervera (Cytomed facility), Frederic Brau (IMPC) and Nadir Djerbi (PICMI) for technical help, Dr Dominique WEIL, Dr Michel Kress, and Dr Franck Delaunay for plasmid kind gifts.

Abbreviations

MAPK: Mitogen-activated protein kinase

MEKi : MEK inhibitors

PBs: Processing Bodies

RBP: RNA binding proteins

405 LLPS: Liquid Liquid phase separation

406 DMEM: Dulbecco's Modified Eagle Medium

407 FBS: fetal bovine serum

408 RPMI: Roswell Park Memorial Institute

409 siRNA: small interfering RNA

410 SDS: Sodium Dodecyl sulfate

411 PBS: Phosphate-Buffered Saline

412 BSA: Bovine serum albumin

413 PD18: PD184352

414 LUAD: Lung Adenocarcinoma

415 SKCM: Skin Cutaneous Melanoma

416 BRCA: Breast Cancer

417 ActD: Actinomycin D

418 Tram: Trametinib

419 .

References

[1] Anderson P, Kedersha N, Ivanov P. Stress granules, P-bodies and cancer. Biochim Biophys Acta - Gene Regul Mech 2015;1849:861–70. https://doi.org/10.1016/j.bbagrm.2014.11.009.

[2] Masuda K, Kuwano Y. Diverse roles of RNA-binding proteins in cancer traits and their implications in gastrointestinal cancers. Wiley Interdiscip Rev RNA 2019;10:1–18. https://doi.org/10.1002/wrna.1520.

[3] Hubstenberger A, Courel M, Bénard M, Souquere S, Ernoult-Lange M, Chouaib R, et al. P-Body Purification Reveals the Condensation of Repressed mRNA Regulons. Mol Cell 2017;68:144-157.e5. https://doi.org/10.1016/j.molcel.2017.09.003.

[4] Khong A, Matheny T, Jain S, Mitchell SF, Wheeler JR, Parker R. The Stress Granule Transcriptome Reveals Principles of mRNA Accumulation in Stress Granules. Mol Cell 2017;68:808-820.e5. https://doi.org/10.1016/j.molcel.2017.10.015.

[5] Banani SF, Lee HO, Hyman AA, Rosen MK. Biomolecular condensates: Organizers of cellular biochemistry. Nat Rev Mol Cell Biol 2017;18:285–98. https://doi.org/10.1038/nrm.2017.7.

[6] Liu J, Valencia-Sanchez MA, Hannon GJ, Parker R. MicroRNA-dependent localization of targeted mRNAs to mammalian P-bodies. Nat Cell Biol 2005;7:719–23. https://doi.org/10.1038/ncb1274.

[7] Pitchiaya S, Mourao MDAA, Jalihal AP, Xiao L, Jiang X, Chinnaiyan AM, et al. Dynamic Recruitment of Single RNAs to Processing Bodies Depends on RNA Functionality. Mol Cell 2019;74:1–13. https://doi.org/10.1016/j.molcel.2019.03.001.

[8] Prior IA, Hood FE, Hartley JL. The frequency of ras mutations in cancer. Cancer Res 2020;80:2669–974. https://doi.org/10.1158/0008-5472.CAN-19-3682.

[9] Anguera G, Majem M. BRAF inhibitors in metastatic non-small cell lung cancer. J Thorac Dis 2018;10:589–92. https://doi.org/10.21037/jtd.2018.01.129.

[10] Awad MM, Liu S, Rybkin II, Arbour KC, Dilly J, Zhu VW, et al. Acquired Resistance to KRAS G12C Inhibition in Cancer . N Engl J Med 2021;384:2382–93. https://doi.org/10.1056/nejmoa2105281.

[11] Tanaka N, Lin JJ, Li C, Ryan MB, Zhang J, Kiedrowski LA, et al. Clinical Acquired Resistance to KRAS G12C Inhibition through a Novel KRAS Switch-II Pocket Mutation and Polyclonal Alterations Converging on RAS–MAPK Reactivation . Cancer Discov 2021:1913–23. https://doi.org/10.1158/2159-8290.cd-21-0365.

[12] Smith LK, Sheppard KE, McArthur GA. Is resistance to targeted therapy in cancer inevitable? Cancer Cell 2021;39:1047–9. https://doi.org/10.1016/j.ccell.2021.07.013.

[13] Aldea M, Andre F, Marabelle A, Dogan S, Barlesi F, Soria JC. Overcoming resistance to tumor-targeted and immune-targeted therapies. Cancer Discov 2021;11:874–99. https://doi.org/10.1158/2159-8290.CD-20-1638.

[14] Wang Y, Van Becelaere K, Jiang P, Przybranowski S, Omer C, Sebolt-Leopold J. A role for K-ras in conferring resistance to the MEK inhibitor, CI-1040. Neoplasia 2005;7:336–47. https://doi.org/10.1593/neo.04532.

[15] Ambrosini G, Khanin R, Carvajal RD, Schwartz GK. Overexpression of DDX43 mediates MEK inhibitor resistance through RAS upregulation in uveal melanoma cells. Mol Cancer Ther 2014;13:2073–80. https://doi.org/10.1158/1535-7163.MCT-14-0095.

[16] Feillet C, Krusche P, Tamanini F, Janssens RC, Downey MJ, Martin P, et al. Phase locking and multiple oscillating attractors for the coupled mammalian clock and cell cycle. Proc Natl Acad Sci U S A 2014;111:9828–33. https://doi.org/10.1073/pnas.1320474111.

[17] Zangari J, Ilie M, Rouaud F, Signetti L, Ohanna M, Didier R, et al. Rapid decay of engulfed extracellular miRNA by XRN1 exonuclease promotes transient epithelial-mesenchymal transition. Nucleic Acids Res 2016;45:4131–41. https://doi.org/10.1093/nar/gkw1284.

[18] Lassalle S, Zangari J, Popa A, Ilie M, Hofman V, Long E, et al. MicroRNA-375/SEC23A as biomarkers of the *in vitro* efficacy of vandetanib. Oncotarget 2016;7. https://doi.org/10.18632/oncotarget.8458.

[19] Pillai RS, Bhattacharyya SN, Artus CG, Zoller T, Cougot N, Basyuk E, et al. Inhibition of translational initiation by let-7 microRNA in human cells. Science (80-) 2005;309:1573–6. https://doi.org/10.1126/science.1115079.

[20] Chen Z, Fillmore CM, Hammerman PS, Kim CF, Wong K-K. Non-small-cell lung cancers: a heterogeneous set of diseases. Nat Rev Cancer 2014;14:535–46. https://doi.org/10.1038/nrc3775.

[21] De Conti G, Dias MH, Bernards R. Fighting drug resistance through the targeting of drug-tolerant persister cells. Cancers (Basel) 2021;13:1–15. https://doi.org/10.3390/cancers13051118.

[22] Marin-Bejar O, Rogiers A, Dewaele M, Femel J, Karras P, Pozniak J, et al. Evolutionary predictability of genetic versus nongenetic resistance to anticancer drugs in melanoma. Cancer Cell 2021;39:1135-1149.e8. https://doi.org/10.1016/j.ccell.2021.05.015.

[23] Marine JC, Dawson SJ, Dawson MA. Non-genetic mechanisms of therapeutic resistance in cancer. Nat Rev Cancer 2020;20:743–56. https://doi.org/10.1038/s41568-020-00302-4.

[24] Meyer M, Paquet A, Arguel M-J, Peyre L, Gomes-Pereira LC, Lebrigand K, et al. Profiling the Non-genetic Origins of Cancer Drug Resistance with a Single-Cell Functional Genomics Approach Using Predictive Cell Dynamics. Cell Syst 2020;11. https://doi.org/10.1016/j.cels.2020.08.019.

[25] Vendramin R, Litchfield K, Swanton C. Cancer evolution: Darwin and beyond. EMBO J 2021;40:1–20. https://doi.org/10.15252/embj.2021108389.

[26] Algazi AP, Othus M, Daud AI, Lo RS, Mehnert JM, Truong TG, et al. Continuous versus intermittent BRAF and MEK inhibition in patients with BRAF-mutated melanoma: a randomized phase 2 trial. Nat Med 2020;26:1564–8. https://doi.org/10.1038/s41591-020-1060-8.

[27] Oren Y, Tsabar M, Cuoco MS, Amir-Zilberstein L, Cabanos HF, Hütter JC, et al. Cycling cancer persister cells arise from lineages with distinct programs. Nature 2021;596:576–82. https://doi.org/10.1038/s41586-021-03796-6.

[28] Berchtold D, Battich N, Pelkmans L. A Systems-Level Study Reveals Regulators of Membrane-less Organelles in Human Cells. Mol Cell 2018;72:1035-1049.e5. https://doi.org/10.1016/j.molcel.2018.10.036.

[29] Johnson SM, Grosshans H, Shingara J, Byrom M, Jarvis R, Cheng A, et al. RAS is regulated by the let-7 microRNA family. Cell 2005;120:635–47. https://doi.org/10.1016/j.cell.2005.01.014.

[30] Courel M, Clément Y, Bossevain C, Foretek D, Vidal Cruchez O, Yi Z, et al. GC content shapes mRNA storage and decay in human cells. Elife 2019;8.

https://doi.org/10.7554/eLife.49708.

[31] Fu J, Dang Y, Counter C, Liu Y. Codon usage regulates human KRAS expression at both transcriptional and translational levels. J Biol Chem 2018;293:17929–40. https://doi.org/10.1074/jbc.RA118.004908.

[32] Lampson BL, Pershing NLK, Prinz JA, Lacsina JR, Marzluff WF, Nicchitta C V., et al. Rare codons regulate KRas oncogenesis. Curr Biol 2013;23:70–5. https://doi.org/10.1016/j.cub.2012.11.031.

Figure legends

Figure 1. MEKi treatments induce potent KRAS and NRAS overexpression in cancer cells.

A. Cancer cells were treated 24h with PD184352 (PD18) and trametinib (Tram) at 10µM and 10nM respectively. LUAD: Lung Adenocarcinoma; SKCM: Skin Cutaneous Melanoma; BRCA: Breast Cancer **B.** A549 cells were transfected with the indicated siRNAs for 24h followed by 24h of treatment with PD184352 at 10µM (PD18). **A-B.** Western blot analysis of the indicated proteins. pERK and pBRAF represents phosphorylated form of ERK and BRAF respectively Results are representative of 3 independent experiments.

Figure 2. KRAS and NRAS overexpression is dependent on increased translation.

A-B. A549 cells were treated with PD184352 (PD18) at 10µM and harvested at 24h. mRNA expression analysis of the indicated genes were analyzed by RT-qPCR using RPLP0 for normalization and untreated (Ctl) as reference. Results represent the combination of 3 independent experiments. A Mann-Whitney test was performed for statistical analysis. (n.s.: non-significative) **C.** A549 cells were treated with PD184352 (PD18) at 10µM and Actinomycin D (ActD) at 1µg/mL and harvested at the indicated time. Western blot analysis of the indicated proteins. Results are representative of 3 independent experiments. **D.** Polysome profiles (grey) of A549 cells treated 24h with PD184352 (PD18) at 10µM. One representative profile from two independent experiments is shown. RNA levels (Blue) of indicated transcripts in each polysomal fraction obtained by sucrose-gradient ultracentrifugation was quantified by qRT–PCR. Dotted- line represents baseline.

Figure 3. MEKi treatment is associated with a PBs decrease in size and number.

A-C. A549 cells were treated 24h with PD184352 (PD18) and trametinib (Tram) at 10µM and 10nM respectively. **D-F.** H1650, MEL501, BT549 cells respectively were treated 24h with PD184352 (PD18) and trametinib (Tram) at 10µM and 10nM respectively. **G.H.** A549 cells were treated with PD184352 (PD18) at 10µM and harvested at the indicated time. **A.** Confocal analysis of PBs using anti-DDX6 antibodies (Inverted/green) with DAPI nuclear staining (blue). Results are representative of 3 independent experiments. **B-H.** Quantification of PBs indicated parameters by ImageJ. Results are representative of 3 independent merged experiments with a minimal quantification of 100 cells for each condition. Mann-Whitney test was performed for statistical analysis. For all experiments, the P-value was indicated as *<0.05, **<0.01, ***<0.005. **I.** Western blot analysis of the indicated time. pERK represents phosphorylated form of ERK. Results are representative of 3 independent experiments.

Figure 4. Dynamic regulation of PBs formation and MAPK signaling.

A549 cell were treated with PD184352 (PD18) at 10µM, after 24h MEKi was removed, and cells were harvested at the indicated time. **A.** Scheme of the experiments presented in panel B-D. **B.** Western blot analysis of the indicated time. pERK and pBRAF represents phosphorylated form of ERK and BRAF respectively. Results are representative of 3 independent experiments. **C.D.** Quantification of PBs number and size respectively by ImageJ. Results are representative of 3 independent merged experiments with a minimal quantification of 100 cells for each condition. Mann-Whitney test was performed for statistical analysis. For all experiments, the P-value was indicated as **<0.01; ***<0.005.

E. Cell counts at indicated time. Results are representative of 3 independent biological replicates.

Figure 5. Resistant cells maintain a low PBs phenotype overtime.

A549 wild type (WT) cells and 2.5 µM PD18 resistant cells (PD18_R) were treated 24h with PD184352 (PD18) at 2.5µM or at 10µM. **A.** Western blot analysis of the indicated time. pERK represents phosphorylated form of ERK. Results are representative of 3 independent experiments. **B.C.** Quantification of PBs number and size respectively by ImageJ. Results are representative of 3 independent merged experiments with a minimal quantification of 100 cells for each condition. A Mann-Whitney test was performed for statistical analysis. For all experiments, the P-value was indicated as *<0.05; **<0.01; ***<0.005.

Figure 6. DDX6 expression controls KRAS and NRAS translation.

A-E. A549 wild type (WT) cells, overexpressing a green fluorescent protein (GFP) and a DDX6-GFP fused protein (DDX6). **F.G**. A549 cells were transfected with a siControl (siCTL) or with a siDDX6 for 48h. **A.F.** Western blot analysis at the indicated time. Results are representative of 3 independent experiments. **B.C.G.** Quantification of PBs number and/or size by ImageJ. Results are representative of 3 independent merged experiments with a minimal quantification of 100 cells for each condition. A Mann-Whitney test was performed for statistical analysis**. D.E.** A549 wild type (WT) cells, overexpressing a DDX6-GFP fused protein. mRNA expression analysis of the indicated genes was analyzed by RT-qPCR using RPLP0 for normalization and untreated (WT) as reference. Results represent the combination of 3 independent experiments. A Mann-Whitney test was

performed for statistical analysis. (n.s.: non-significative). For all experiments, the P-value was indicated as *<0.05; **<0.01; ***<0.005.

Supplementary Figure 1.

A549 cells were pretreated with MG132 at 2.5µM and treated with PD184352 (PD18) at 10µM and harvested at the indicated time. Western blot analysis of the indicated proteins. Results are representative of 3 independent experiments.

Supplementary Figure 2.

A. H1650, **B.** MEL501 and **C.** BT549 cells were treated 24h with PD184352 (PD18) or trametinib (Tram). **D.E.** A549 cells were treated with PD184352 (PD18) at 10µM and harvested at indicated time. **A-D.** Confocal analysis of PBs using anti-DDX6 antibodies (inverted color/green) with DAPI nuclear staining (blue). **E.** Cell cycle distribution was analyzed by flow cytometry. Results represent the merge of 3 independent experiments.

Supplementary Figure 3.

A549 cells were treated 24h with PD184352 (PD18) at 10µM and 20min with Sodium Arsenite ($NaAsO_2$) at 0.5mM. Confocal analysis of PBs using anti-DDX6 (Inverted/green) and stress granule anti-G3BP1 (Inverted/red) antibodies respectively with DAPI nuclear staining (blue).

Supplementary Figure 4.

A549 cells were treated with PD184352 (PD18) at 10µM, after 24h MEKi was removed, and cells were harvested at the indicated time. Confocal analysis of PBs using anti-DDX6 (Inverted/green) antibodies with DAPI nuclear staining (blue).

Supplementary Figure 5.

A. A549 wild type (WT) cells and 2.5µM PD18 resistant cells (PD18_R) were treated 24h with PD184352 (PD18) at indicated concentrations. Confocal analysis of PBs using anti-DDX6 (Inverted/green) and LSM14A (Inverted/Red) antibodies with DAPI nuclear staining (blue). **B**. Resistant cells (PD18_R) were cultured in absence or in presence of PD184352 (2.5 µM) and counted at indicated time. Results are representative of 3 independent biological replicates.

Supplementary Figure 6.

A. A549 wild type (WT) cells, overexpressing a green fluorescent protein (GFP) and a DDX6-GFP fused protein (DDX6). **B.** A549 cells were transfected with a siControl (siCTL) or with a siDDX6 for 48h. **A-B.** Confocal analysis of PBs using anti-LSM14 (Inverted/green) antibodies with DAPI nuclear staining (blue).

Supplementary Figure 7.

Negative feedback loop under ERK1/2 phosphorylation is associated with Processing bodies (PBs) formation. PBs control *KRAS* and *NRAS* mRNA translation. PBs dissolution under MEKi treatment is associated with enhanced *KRAS* and *NRAS* mRNA translation

Supplementary Table

List of reagents

REAGENT or RESOURCE	SOURCE	IDENTIFIER
Antibodies		
AlexaFluor 488 chicken anti-Rabbit IgG	Invitrogen	A21441
AlexaFluor 594 chicken anti-Rabbit IgG	Invitrogen	A21442
Anti-mouse IgG (HRP conjugate)	Promega	W402-B
Anti-rabbit (HRP conjugate)	Promega	W401-B
Anti-tubulin	Sigma	T9026
BRAF (55C6)	Cell Signaling Technology	9433S
DDX6	Bethyl	A300-460A
G3BP1	Santa cruz biotechnology	sc-365338
GAPDH	Cell Signaling Technology	2118L
KRAS	Novus	H00003845
LSM14A	Bethyl	A305-102A-M
NRAS (F155)	Santa Cruz biotechnology	sc-31
p44/42 MAPK (ERK1/2)	Cell Signaling Technology	9102S
P-p44/42 MAPK (pERK)	Cell Signaling Technology	9101S
Chemicals, Peptides, and Recombinant Proteins		
DC™ Protein Assay Kit	BioRad	5000111
Direct-zol RNA MiniPrep Plus	ZymoResearch	R2072
Fast SYBR-Green Master Mix	Applied Biosystems	4385612
High-Capacity cDNA Reverse Transcription Kit	Applied Biosystems	4368814
Paraformaldehyde 32% solution EM grade	Electron Microscopy Science	15714
Prolong Diamond Antifade Mountant with DAPI	Invitrogen	P36962
Protein ladder	Euromedex	06P-0111
RNAse OUT	Invitrogen	10777-019
TaqMan™ Fast Advanced Master Mix	Applied Biosystems	4444965
TaqMan™ MicroRNA Reverse Transcription Kit	Applied Biosystems	4366597
TRI Reagent®	Molecular Research Center	TR 118
Cell culture and treatments		
Puromycin Dihydrochloride	Invitrogen	A1113803
0,05% trypsin-EDTA (1X)	Gibco	25300-054
Actinomycin D	Gibco	11805-017
Amicon Ultra-15, PLHK, 100 kD	Sigma-aldrich/Merck	UFC9100024
DDX6 silencer select	Ambion	4392420 (id : s4010)
Dimethyl-sulfoxide	Sigma-aldrich/Merck	276855-100mL
DMEM (1X) + Glutamax-I	Gibco	31966-021
Jet Prime transfection reagent	Polyplus	114-15
KRAS silencer select-validated	Ambion	4390824 (id : s7940)

Lipofectamine 3000	Invitrogen	L3000-008
LSM14A silencer select	Ambion	4392420 (id : s25051)
MEM NEAA	Gibco	11140-35
MG132	Tocris	1748
Negative Control siRNA #1 Silencer Select	Ambion	4390843
NRAS silencer select-validated	Ambion	4390824 (id : s55)
PD184352	Sigma-aldrich/Merck	P30181-5mg
Polybrene Infection / Transfection Reagent	Sigma-aldrich/Merck	TR-1003-G
RPMI Medium 1640 (1X) + Glutamax-I	Gibco	61870-010
Sodium Arsenite Solution	Supelco	106277
Trametinib	TargetMOI	TA-T2125-5mg
Oligonucleotides		
KRAS-Forward	GACTGGGGAGGGCTTTCTTT	
KRAS-Reverse	GCATCATCAACACCCTGTCT	
NRAS-Forward	CCAATACATGAGGACAGGCGA	
NRAS-Reverse	TCACACTTGTTTCCCACTAGCA	
RPLP0-Forward	GCATCAGTACCCCATTCTATCAT	
RPLP0-Reverse	AGGTGTAATCCGTCTCCACAGA	
Recombinant DNA		
pEGFP-C1_p54cp	Gift	
pPRIPu-CrUCCI	Gift	
Software and Algorithms		
CytExpert 2.3		
ImageJ 1.53j		
Prism 8.0.2		
StepOne Software v2.3		

649

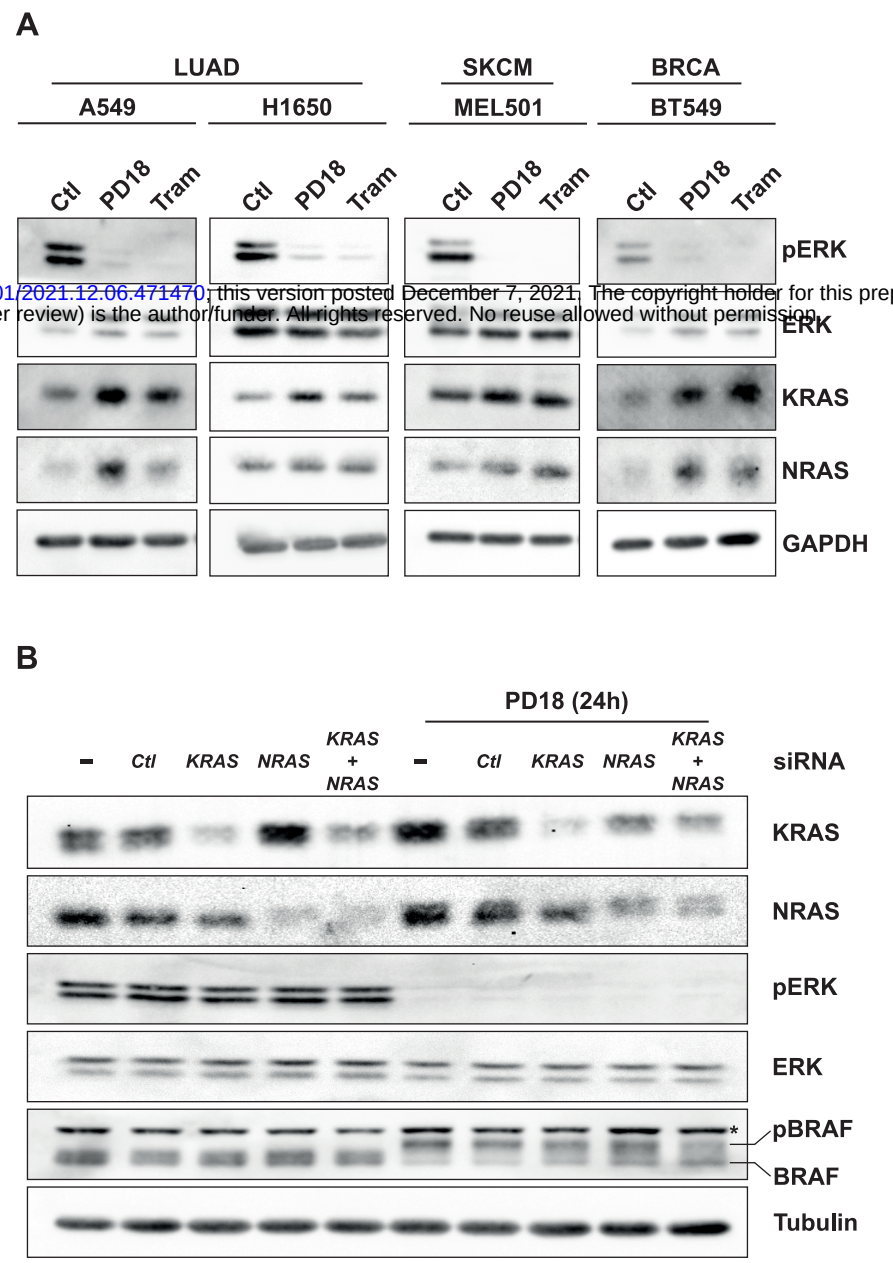

Figure 1

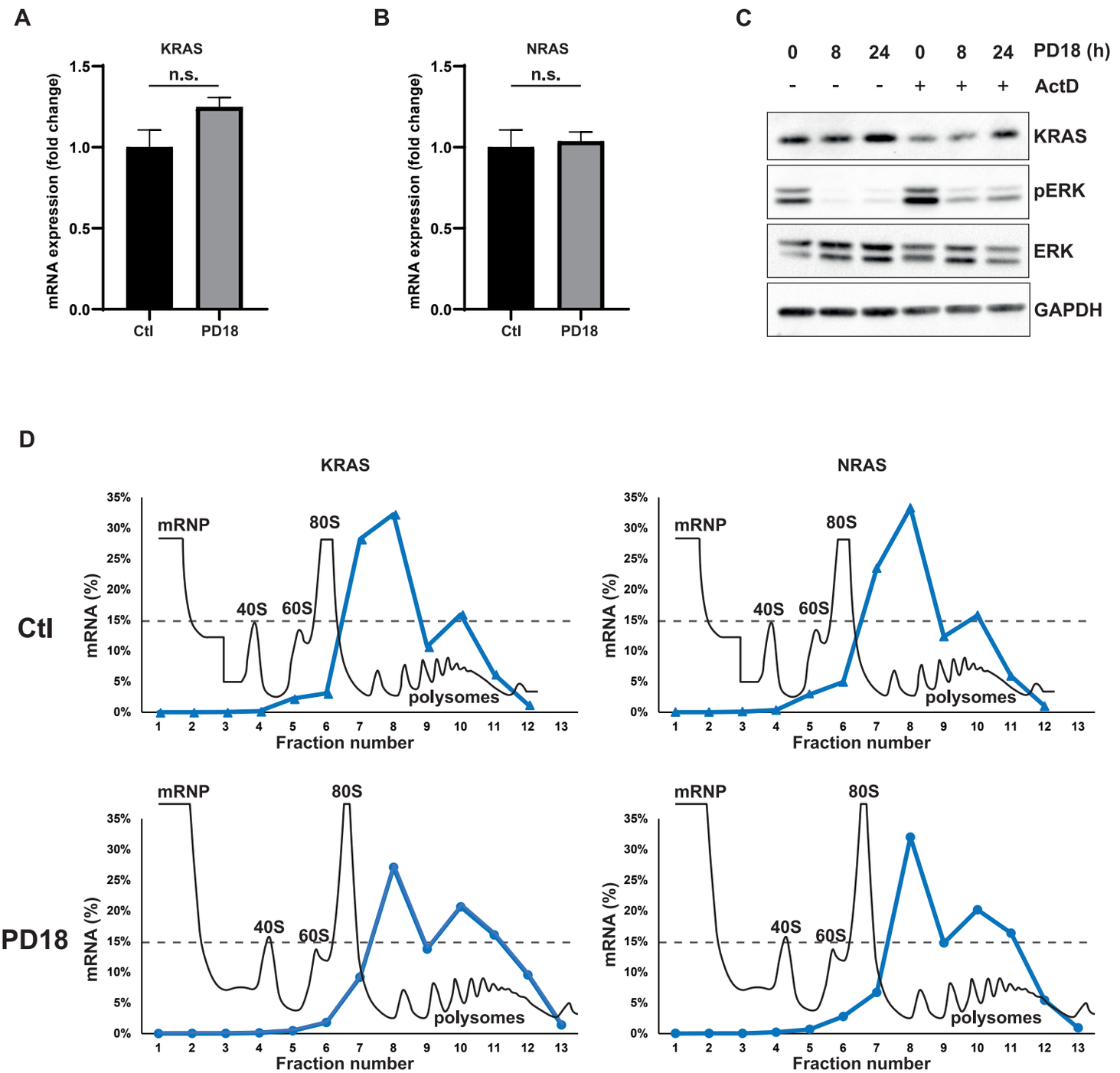

Figure 2

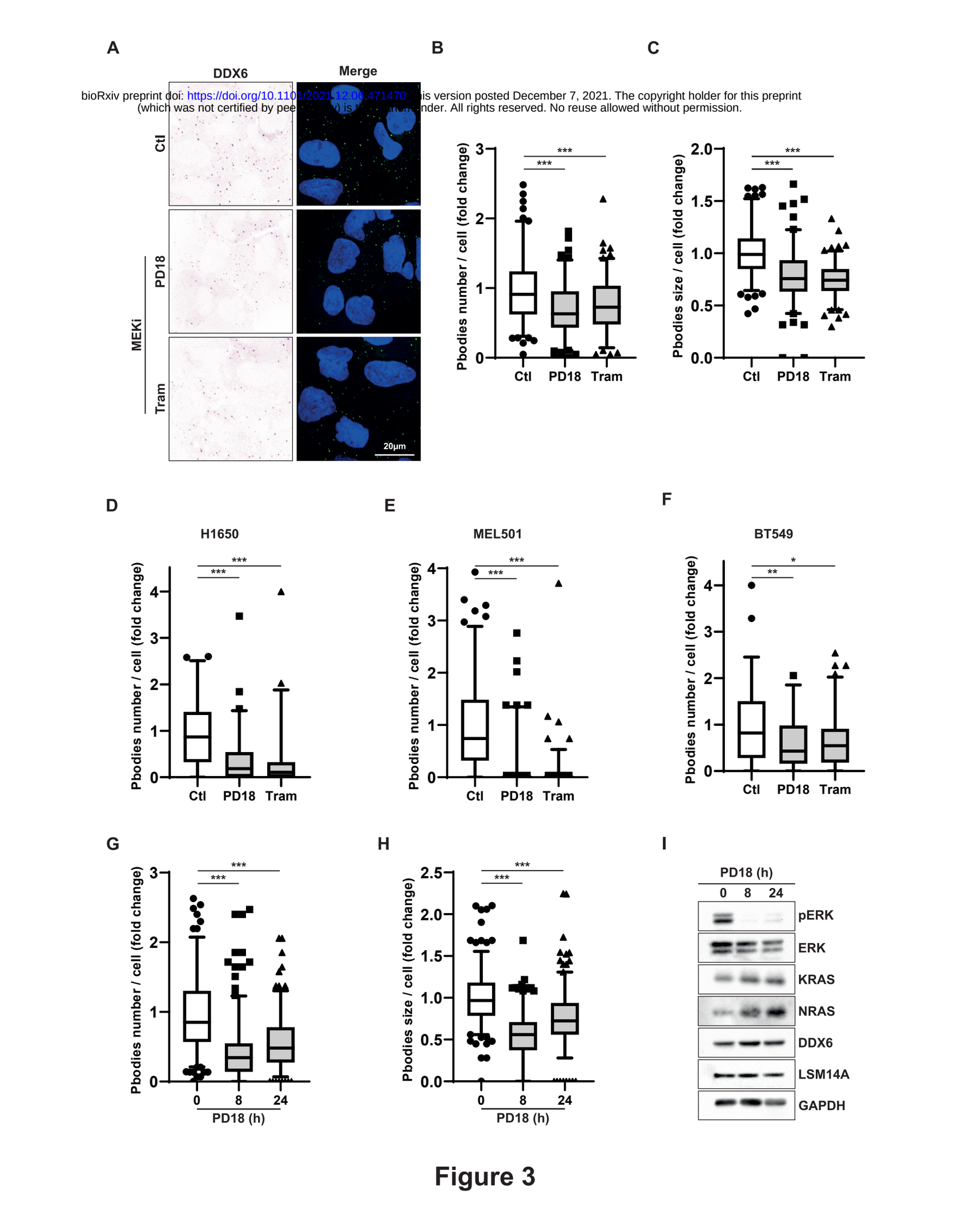

Figure 3

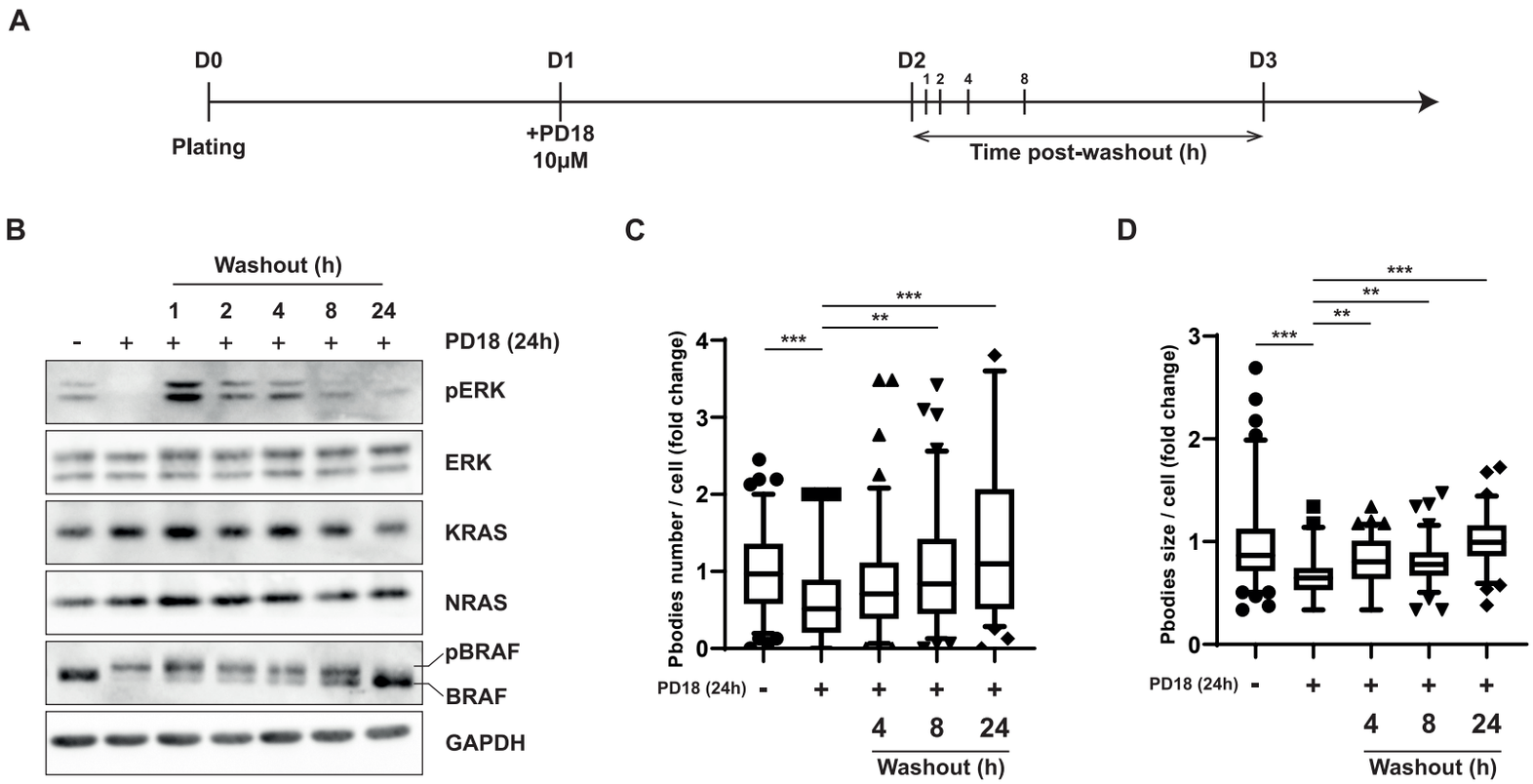

Figure 4

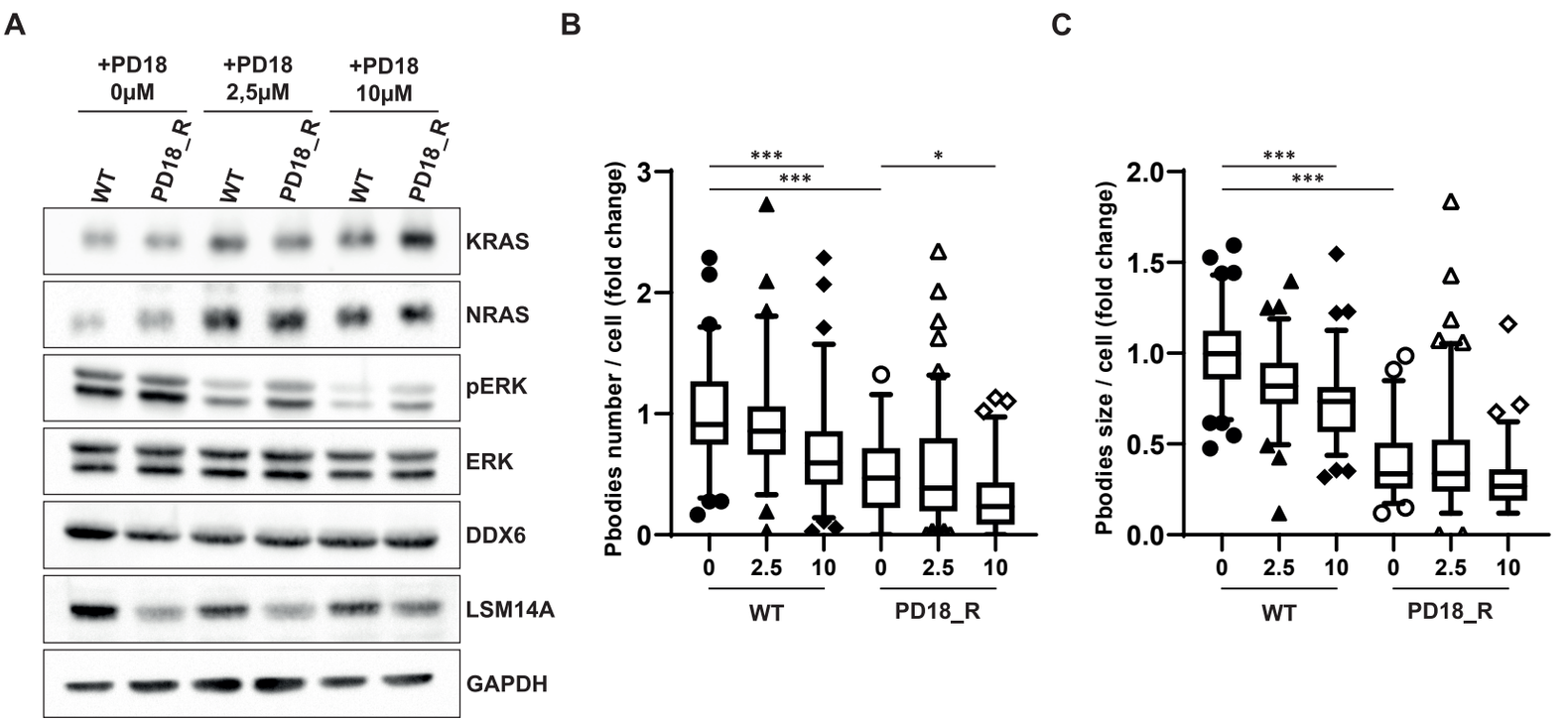

Figure 5

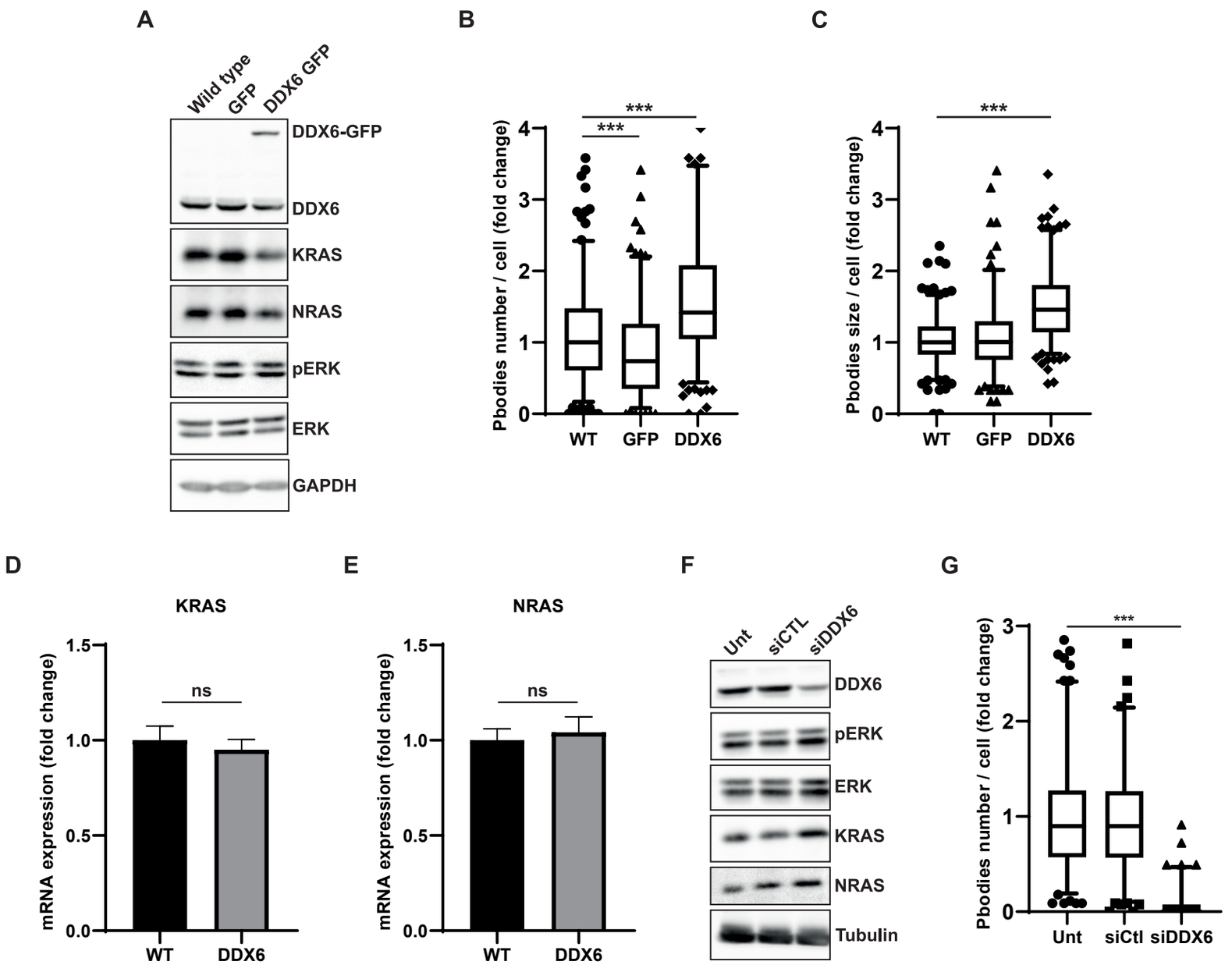

Figure 6